INTERNATIONAL JOURNAL OF ROBOTICS
(THEORY AND APPLICATIONS)
E-mail: IJR@kntu.ac.ir

Modeling and Sensitivity Analysis of Stick-Slip Piezoelectric Rotary Inertia Motor

M. Azadkhani[a], F. Karimi[a], H. Ghafarirad[a,*] and M. Zareinejad[b]

[a] Faculty of Mechanical Engineering, Amirkabir University of Technology, Tehran, Iran, P.O. Box, 159163-4311
[b] New Technologies Research Center, Amirkabir University of Technology, Tehran, Iran, P.O. Box, 159163-4311

ARTICLEINFO

Article history:
Submit: 2024-06-18
Revise: 2024-09-20
Accept: 2024-09-22

Keywords:
Rotary Piezomotor
Stick-Slip Motion
Sensitivity Analysis
Compliant Mechanism

ABSTRACT

This paper presents a comprehensive investigation of piezoelectric inertia motors. The study progressed with the meticulous fabrication of arotational piezomotor, allowing for empirical data collection. A mathematical model was then developed, and system parameters were identified. A comparative analysis revealed significant improvements in model accuracy when LuGre friction was employed, reducing the root mean square error (RSME) by approximately six-fold compared to previous models using Coulomb friction. Following model validation, a sensitivity analysis assessed the impact of parameter variations—specifically voltage, frequency, friction coefficient, and duty ratio—on the motor's performance. It provides valuable insights into how the physical parameters influence the motor's movement. Results indicated that the duty ratio had the most substantial effect on rotor speed, followed by frequency and voltage, while an inverse relationship was found between the friction coefficient and rotational speed.

* Corresponding address: Amirkabir University of Technology, Tehran, Iran,
Tel.: +98-21-64543422; fax: +98-21-66419736.
E-mail address: Ghafarirad@aut.ac.ir

1. Introduction

Piezoelectric motors are widely employed across diverse fields such as micro-electronics, precision manipulation and positioning [1], micro-nano robotics, and ultra-precise microscopes [2]. These motors are favored for their compact size, rapid response, and precise control [3]. They operate by converting voltage into displacement through the reverse piezoelectric effect. While these mechanisms are well-suited for high-precision positioning and maneuverability [4], their limited range of motion led to the development of piezoelectric motors to enhance performance through integration with various systems.

Piezoelectric motors can generally be classified into four types based on their working mechanisms: stepping, inertial, standing wave, and traveling wave [5]. Among these, standing wave and traveling wave motors operate at ultrasonic frequencies, which is why they are commonly referred to as ultrasonic piezoelectric motors. Ultrasonic piezoelectric motors rely on the resonance of the stator, which presents significant challenges in maintaining optimal performance. Deviations from the resonant frequency, often caused by environmental factors such as temperature and humidity, lead to reduced efficiency and inconsistent operation. Furthermore, maintaining the proper preload between the stator and rotor is critical but difficult—insufficient preload can result in slipping, which reduces output force and precision, while excessive preload increases wear, and energy consumption, and shortens the motor's lifespan [6]. Ultrasonic planar piezoelectric motors, a subtype of ultrasonic motors, experience significant wear due to their reliance on dynamic friction forces. The repeated contact between the driving components and surfaces leads to friction-induced material degradation, reducing both accuracy and the motor’s overall precision over time, particularly in high-precision applications [7].

Walking-type or stepping piezoelectric motors, on the other hand, typically involve complex designs with multiple piezoelectric elements and intricate structures, such as clamping and driving units. This complexity increases the challenges in manufacturing, as precise fabrication and accurate assembly are crucial for mechanical stability and performance. Additionally, sophisticated controlsystems are required to coordinate multiple voltage inputs for clamping and driving actions. Despite these advances, walking-type motors often exhibit limitations in force output and response frequency [8][9].

In contrast, piezoelectric inertia motors offer several advantages, including substantial output displacement, high force output, and excellent resolution, making them particularly attractive for various applications. This paper focuses on stick-slip rotary piezoelectric actuators, a widely used configuration in both linear and rotary piezoelectric motor designs [10].

In the articles presented in the field of rotary piezoelectric motors, most efforts have been directed toward developing piezoelectric motors by introducing new models. There have been fewer attempts to identify the impact of parameters and improve existing structures. Some research has aimed to address this issue, for example, Heading et al. investigated a piezoelectric motor, highlighting its potential for rapid positioning. They explored novel actuator concepts, achieving significant speed enhancements, albeit facing challenges in preload control. Their study underscores the need for advanced control strategies and dynamic performance metrics to optimize actuator output power effectively [11]. Lu et al. introduce a stick-slip motor with asymmetrical compliant mechanisms, demonstrating oblique motion. Their study proposes an MDR friction model and utilizes FEM analysis to optimize actuator dimensions, enhancing output performance. Experimental validation confirms model accuracy, highlighting the actuator's versatility and efficiency in motion control applications [12]. Yang et al. created a method for optimizing topology for a piezoelectric stick-slip motor, converting vertical to oblique displacement via a flexure hinge mechanism. Their optimized design, verified by finite element analysis and experimental tests, achieved a velocity of 15.25 mm/s and a resolution of 96 nm. This study demonstrates the method's effectiveness in improving actuator performance [13]. José et al. conducted a sensitivity analysis and optimization of an ultrasonic linear piezo motor using design of experiments and FEM. The study successfully increased the deformation amplitude of the motor by over ten times compared to the initial design. The research underscores the importance of sensitivity analysis and feasibility studies in the design and optimization of smart ultrasonic actuators.[14] Dong et al. presented an optimal design of an ultrasonic motor using a combination of FEM, sensitivity analysis, and adaptive genetic algorithm. This method not only solved the difficulty of multi-objective optimization but also improved optimization efficiency and accuracy. The performance of the optimized motor was significantly improved after optimization [15]. Tiemin et al. developed a new piezoelectric motor, addressing the conflict between positioning accuracy and speed in the rapidly evolving chip packaging industry. Through FE analysis and optimization process, they demonstrated how the geometry, material properties, and boundary conditions of the oscillator influence the vibration

modal of the stator [16]. Flueckiger et al. developed a design methodology for piezoelectric ultrasonic motors, combining sensitivity analysis and finite element method (FEM) based optimization algorithms. This approach maximizes vibration amplitude, reduces calculation time, and narrows the variation range of significant parameters. The methodology was validated through the creation and testing of functional motor models, with future work suggested to include a full 3D FEM model considering the contact phenomenon between stator and rotor [17].

Upon reviewing the literature, a research gap was identified: the lack of studies that combine precise mathematical modeling with sensitivity analysis of models employing stick-slip operation. While previous studies have conducted a sensitivity analysis using finite element methods, this paper utilizes an analytical approach. This research represents a significant advancement in the control and optimization of rotary piezoelectric motors utilizing stick-slip operation.

2. Motor Structure

The motor configuration outlined in this manuscript in Figure 1, showcases a flexible rhombic mechanism that contains piezoelectric ceramic within itself.

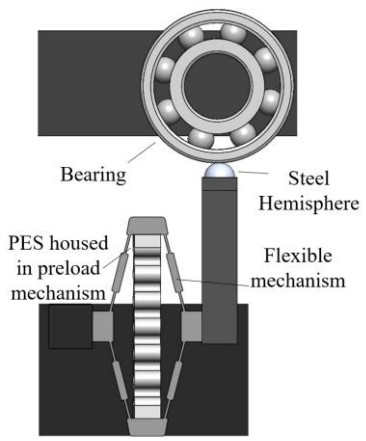

Fig. 1. Model of the designed prototypepiezoelectric motor

2.1. Piezoelectric ceramic

In this research, the Piezo Stack Actuator (SA050536) was selected as the piezoelectric ceramic due to its well-documented performance characteristics. With a length of 36 millimeters and a stiffness of 28 N/µm.

2.2. Input voltage

For a piezoelectric motor to operate, it must be propelled forward by a contact point. This propulsion occurs through an increase in voltage. As illustrated in Figure 2-b When the voltage is elevated, the length of the piezoelectric ceramic expands, resulting in the elongation of the major axis of the rhombus. Consequently, this elongation causes the minor axis of the rhombus to contract, thereby moving the contact point to the left. The voltage increase must be gradual enough to allow the mechanism to stick to the rotor, which is crucial for the bearing drive in the piezoelectric traveling motor.

Subsequently, when the voltage decreases as shown in Figure 2-c, the length of the piezoelectric ceramic contracts and the major axis of the rhombus mechanism shortens. As a result, the minor axis of the rhombus elongates, returning to its original position. The return movement occurs more rapidly, enabling the contact points to slip over one another.

Overall, this stick-slip movement comprises a combination of forward and backward motions. Given that the forward movement is slower, its magnitude is greater, leading to a net forward motion. Alternative voltages can be calculated using the equation provided below. The ratio of the time taken for the voltage to increase to the time taken for the voltage to decrease is called the duty ratio.

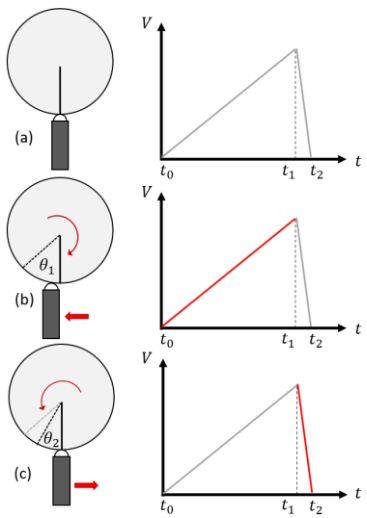

Fig. 2motion procedure of the rotary piezo moto

In equation 1, the function of generation of the sawtooth wave is illustrated, the $\frac{V_0 t}{C_{dr} T e_{dr}}$ is slope of the sawtooth wave and C_{dr} is coefficient of duty ratio.

$$V = \begin{cases} \frac{V_0 t}{C_{dr} T e_{dr}} \frac{t}{T} - \left[\frac{t}{T}\right] < C_{dr} T e_{dr} \\ \frac{V_0 (t-T)}{(1 - C_{dr} e_{dr}) T} \frac{t}{T} - \left[\frac{t}{T}\right] > C_{dr} T e_{dr} \end{cases} \quad (1)$$

Also, T is set equal to $1/fr$, where fr represents frequency, and $e_{dr}$is a parameter estimating the error in generating the input wave.

2.3. Pre-load Structure

To maintain consistent pressure on piezoelectric ceramics and safeguard against potential harm from stretching forces, a pre-load system has been integrated into the motor structure. In this setup, the ceramic part sits inside a pre-load enclosure, securely held in place on both sides by screws attached to a compliant mechanism.

2.4. Flexure Mechanism

Given the restricted displacement capacity of piezoelectric materials, flexure mechanisms are frequently utilized in the majority of piezoelectric actuators. Flexible mechanisms are employed to enhance the efficiency of piezoelectric motors. These mechanisms leverage geometric relationships to amplify the range of motion of the piezoelectric ceramic.

2.5. Rotor

In the piezoelectric motor showcased, a 62202-2RS1 SKF bearing has been employed to enhance performance and reliability. The 62202-2RS1 is a deep groove ball bearing with a bore diameter of 15 mm, an outer diameter of 35 mm, and a width of 14 mm.

3. Mathematical Modeling and simulation

For mathematical modeling, it is essential to simplify the problem statement. A critical aspect of this model for the piezoelectric motor is accurately representing the contact between two moving bodies. This is vital because the operation of stick-slip piezoelectric motors fundamentally relies on the friction between surfaces.

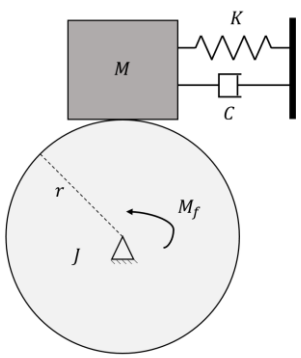

Fig. 3. The Rotary piezoelectric motor schematic model

Depicted in Fig. 3, the model consists of two discrete masses. Firstly, denoted as M, it encompasses the mass of the piezoelectric ceramic, measuring 7.17 grams, and the magnification mechanism's mass, totaling 14.53 grams. Combined, M sums up to 21.7 grams. The second mass, J, is derived through software after importing its CAD file, calculated to be $4.48 \times 10^{-6}\ [kg.m^2]$. Through the integration of these elements, the proposed model adeptly encapsulates the motor's dynamic behavior.

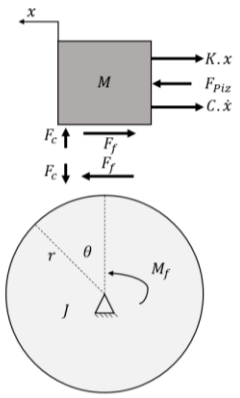

Fig. 4. Rotary piezoelectric motor free body diagram

In mathematical modeling, the first step is to spatially separate items and create a thorough free-body diagram. The force acting on an M is represented by the following equation:

$$M\ddot{x} + C\dot{x} + Kx = F_{pes} - F_f \qquad (2)$$

And for rotor :

$$J\ddot{\theta} = M_f \qquad (3)$$

The frictional force arising between the flexible mechanism and the rotor induces a torque within the rotor, manifested as follows:

$$M_f = rF_f \qquad (4)$$

In order to determine the frictional force, it is imperative to evaluate the relative velocity between two surfaces. To achieve this, the linear velocity can be obtained by multiplying the radius by the angular velocity.

$$\dot{x} = r\dot{\theta} \qquad (5)$$

The characterization of the frictional force between the interacting surfaces of the driving object and the rotary plate is accomplished through the utilization of the LuGre model [18]. Here, 'x' represents the relative displacement, while 'z' signifies the elastic phase of the pre-sliding displacement. This model provides a comprehensive framework for understanding the intricate dynamics at play, offering valuable

insights into the behavior of the stick-slip piezoelectric motor.

$$F_f = \sigma_0 z + \sigma_1 \frac{dz}{dt} + \sigma_2 \dot{x}$$
$$\frac{dz}{dt} = x(1 - \frac{\sigma_0}{|F_c|} sgn(\dot{x})\, z) \quad (6)$$
$$F_c = \mu F_N$$

In this equation, σ_0 denotes the contact stiffness, while σ_1 representing the damping associated with tangential compliance. Additionally, σ_2 signifies the coefficient governing viscous friction. F_c corresponds to the Coulomb frictional force, F_N denotes the normal force, and μ stands for the coefficient of friction. These parameters collectively provide a comprehensive framework for analyzing the dynamic interplay of forces within the system under examination.

4. Experimental Result

4.1. Experimental Setup

The experimental diagram depicted in Fig. 6 illustrates the connection of the rotary piezo motor to a function generator capable of producing sawtooth waves. During the voltage increase phase, these signals are utilized with a duty cycle of 0.95%, and during the voltage decrease phase, they are utilized with a duty cycle of 0.05%. The specific duty cycles of 0.95 and 0.05 were chosen because a 0.95 duty cycle is commonly used in piezoelectric motor applications to achieve the necessary driving stick-slip behavior. This ratio ensures that the forward motion is slow enough to maintain contact while the return motion remains rapid, facilitating efficient motor operation. The signal received from the function generator will be amplified 20 times by the piezoelectric driver, increasing the input voltage from 4V to 80V. This amplification improves the piezo actuator's ability to generate larger displacements and higher forces. Subsequently, the voltage will be converted to displacement by the piezoelectric motor. The displacement will then be measured by a laser displacement sensor, and the data will be sent to the Data Acquisition card (DAQ). Finally, the data can be read in MATLAB/Simulink.

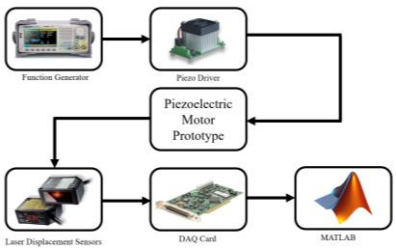

Fig. 5Schematic diagram of the experimental setup

Figure 6 illustrates an overview of the equipment used in this article.

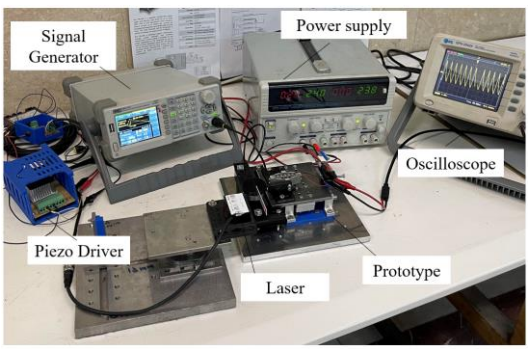

Fig. 6Comprehensive Overview of the Prototype

Figure 7 provides a detailed perspective of a rotary piezoelectric motor, showcasing the interaction between a steel hemisphere and the bearing housing. Additionally, a steel strip is linked to the bearing, with its displacement meticulously measured by a laser displacement sensor.

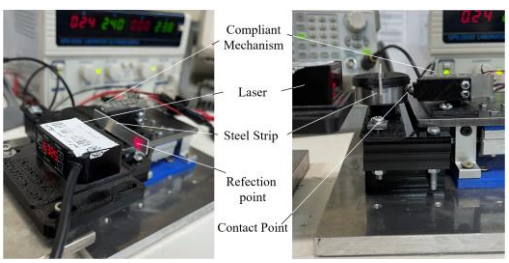

Fig. 7Detailed view of the prototype

To measure the displacement of the piezo motor, which is approximately 400 micrometers, a laser displacement sensor is used. Since the displacement is small, a linear approximation can be employed. The sensor measures displacement based on the reflection point of the laser on the rotor. Due to the geometry of the setup, specifically the ratio between the distance of the laser reflection point and the bearing radius, the displacement measured by the sensor (d_2) is approximately 800 micrometers.

To minimize measurement errors and enhance accuracy, the laser reflection point is positioned farther from the rotor's center ($r_2 = 62\, mm$). This adjustment reduces the proportion of displacement

relative to the rotor's radius, improving the precision of the measurement. The significance of the ratio 77, which represents the displacement-to-radius ratio at the reflection point ($\frac{r_2}{d_2}$), is that it ensures the measured displacement is proportionally small compared to the radius. This helps to minimize any errors introduced during the measurement process.

Furthermore, the larger the ratio ($\frac{r_2}{d_2}$), the more precise the linear motion approximation becomes. However, due to certain design limitations—specifically, that using a larger reflector increases the prototype's dimensions and mass—a suitable reflector length was chosen to balance accuracy and practicality.

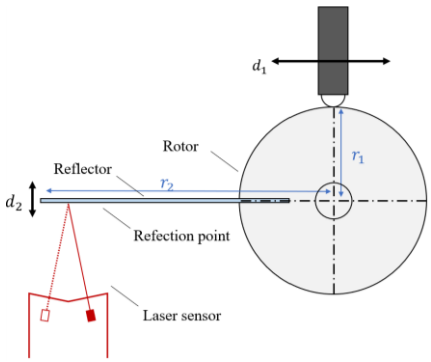

Fig. *8*. Determining the displacement diagram

4.2. Results

The experimental findings showcased in Figure 9 encompassed the motor being operated at two distinct frequencies: 10 Hz and 20 Hz. During these trials, the range of motion was meticulously measured to be 10 milli radians. Remarkably, at a frequency of 10 Hz, the motor completed its motion over a duration of 4.9 seconds, whereas at 20 Hz, the time significantly decreased to 1.36 seconds. These observations offer valuable insights into the motor's performance across varying operating frequencies.

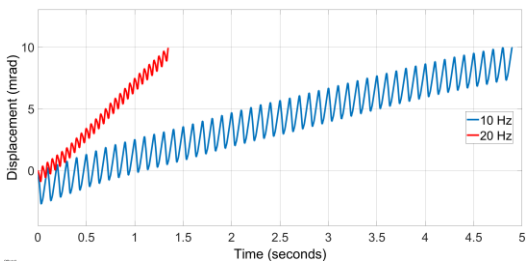

Fig. 9 Experimental results for 10Hz and 20Hz frequency

4.3. System Identification

The integration of the mathematical model into the Simulink software environment has been completed. For reference, a detailed compilation of all model parameters is provided in Table 1.

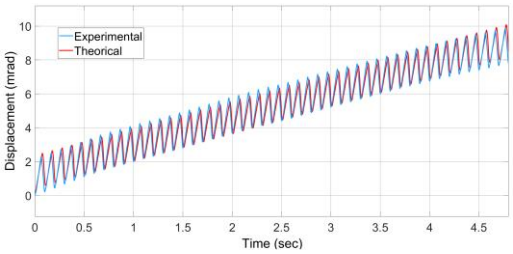

Fig. *10*. Experimental and theoretical data on 10 Hz frequency

In Fig. 10, the blue line illustrates the experimental data collected at a frequency of 10 Hz, whereas the red line depicts the output data derived from the identified model at the same frequency.

Moving to Figure 11, the data originally depicted in Figure 10 is presented within a narrower range. This adjustment aims to accentuate the evident disparity between the experimental and theoretical data. By narrowing the range, a clearer visualization of the difference between the experimental and theoretical datasets is achieved.

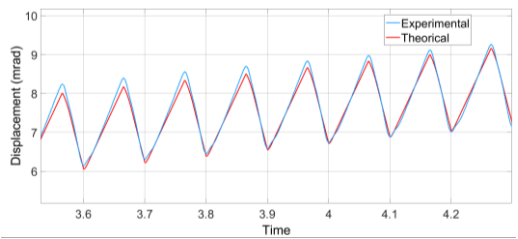

Fig. *11*.Data at 10 Hz within a narrower range.

To evaluate the system's performance at a frequency of 20 Hz, a simulation was executed, and the outcomes are showcased in Figure 12. It's worth emphasizing that our friction model is integral to this analysis. Consequently, as the frequency rises, the magnitude of error also increases, owing to the inherent constraints of the friction model.

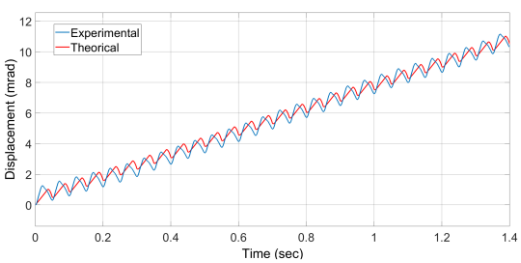

Fig. *12* Experimental and theoretical data on 20 Hz frequency

As depicted in Figure 12, as the frequency increases, so does the error in predicting the behavior of the piezoelectric model. This increasing error can be attributed to several factors.

Firstly, predicting dynamic friction is inherently challenging due to its complex and non-linear nature. The friction model used in this study, while effective at lower frequencies, may not fully capture the dynamic behavior at higher frequencies.

Secondly, the limitations of the numerical methods employed in the simulation could also contribute to the observed discrepancies. Numerical integration errors, discretization errors, and assumptions made during the modeling process can all impact the accuracy of the simulation results.

Table 1 showcases the system parameters that have been meticulously identified. These parameters underwent a rigorous process of experimentation and fine-tuning. Noteworthy among the experimental observations was the discerned inverse correlation between the system's frequency and voltage, coupled with a consequent reduction in the oscilloscope reading. As a result, distinct force values were delineated for frequencies of 10 Hz and 20 Hz.

TABLE I-System parameters

Parameter	Value	determine
V	80 $[volt]$	Imported
e_{dr}	0.789	Identified
$d_{e_{10Hz}}$	0.55 $[\mu m/V]$	Identified
$d_{e_{20Hz}}$	0.228$[\mu m/V]$	Identified
M	21.7×10^{-3} $[Kg]$	Determined
e_{dr}	0.789	Identified
J	4.48×10^{-6} $[kg.m^2]$	Determined
C	20 $[Ns/m]$	Identified
K	28 $[N/\mu m]$	Ref. [19]
r	17.5 [mm]	Determined
μ	0.1	Identified
F_N	4.93×10^{-3} $[N]$	Identified
σ_0	1650 $[N/m]$	Identified
σ_1	40 $[Ns/m]$	Identified
σ_2	0.0001 $[Ns/m]$	Identified

4.4. Comparison of two models

In the study by Azadkhani et al., it was suggested that utilizing a more sophisticated friction model could enhance the accuracy of predicting the motion of piezoelectric motors, particularly at higher frequencies. Following the implementation of a new friction model, it became imperative to assess and compare the errors between two models [20]. Model 1 employed the Coulomb friction model, while Model 2, the friction model utilized in our study, adopted the LuGre friction model. To facilitate a comprehensive comparison, we employed the Root Mean Square Error (RMSE), defined as follows:

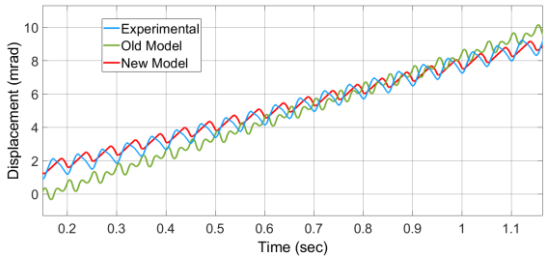

Fig13. Comparison between Coulomb-based model and LuGre-based model

The RMSE was calculated by evaluating the deviations at each position of the piezoelectric motor between experimental and theoretical values under a frequency of 20 Hz. The resulting diagram is presented below.

$$RSME = \sqrt{\frac{1}{n}\sum_{i=1}^{n}(\theta_{Exprimental_i} - \theta_{Theorical_i})^2} \quad (7)$$

As shown, the RMSE significantly improved in Model 2 compared to Model 1. The RMSE of Model 1 was calculated to be 0.35, whereas for Model 2, it was 2.36. This represents a notable enhancement in accuracy. Specifically, the RMSE in Model 2 was approximately 6.59 times better than that of Model 1.

TABLE III-Comparison between 2 models at 20 Hz

RSME Molde 1	RSME Model 2	improvement
2.362	0.358	84.4%

The LuGre model offers several advantages over the Coulomb model, which contributes to its higher precision. The LuGre model incorporates both static and dynamic friction components, allowing it to more accurately represent the frictional behavior of piezoelectric motors. This is particularly important at higher frequencies where dynamic effects become more pronounced.

5. Sensitivity Analysis

Understanding the intricate interplay of voltage, frequency, friction coefficient, and duty ratio on mean velocity is pivotal in optimizing the performance of rotary piezoelectric motors. To delve into this relationship, we systematically varied each parameter by ±10% from its initial value, allowing us to gauge the system's sensitivity.

Our methodology involves calculating the final position of the rotor and dividing it by the runtime of 4.8 seconds to derive the mean velocity. This

standardized approach facilitates a comparative analysis across different parameter variations.

5.1. Voltage

Voltage emerges as a pivotal determinant in the efficiency and performance of rotary piezoelectric motors. In this section, we delve into the sensitivity analysis of voltage, scrutinizing its impact on rotor displacement and mean velocity. Employing five distinct voltage levels—72V, 76V, 80V, 84V, and 88V—we meticulously observe the motor's response to incremental voltage changes of 10% from the baseline of 80V.

Figure 14 visually encapsulates the relationship between voltage and rotor displacement, offering a tangible depiction of the motor's responsiveness to varying input voltages.

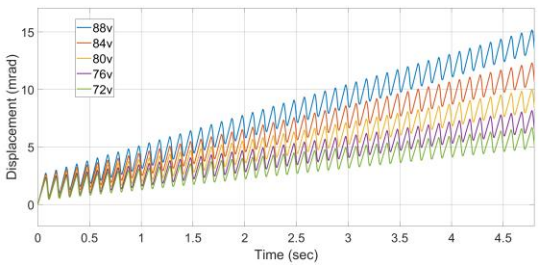

Fig. 14 Displacement corresponding to various voltage levels

This phenomenon is expected because as the applied voltage increases, both the displacement and the generated force of the piezoelectric stack increase. This is directly attributable to the piezoelectric effect, wherein higher voltages induce greater strain in the piezoelectric material, leading to more significant mechanical deformation. Consequently, the rotor displacement rises in response to the enhanced force. Additionally, the torque exerted by the piezoelectric stack grows with increasing voltage, further contributing to the observed displacement.

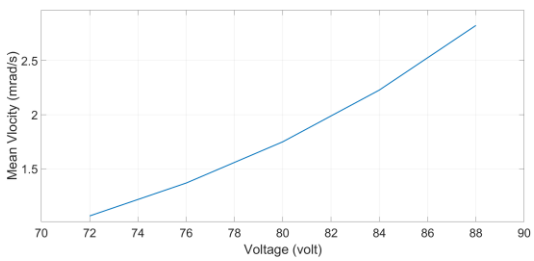

Fig. 15 Mean velocity corresponding to various voltage levels

Figure 15, meanwhile, elucidates the direct correlation between voltage levels and motor performance through the depiction of mean velocity. A discernible linear increase in velocity with rising voltage levels underscores the pivotal role of voltage in enhancing motor performance.

This

5.2. Frequency

Frequency stands out as another pivotal parameter shaping the performance characteristics of piezoelectric motors. Our sensitivity analysis of frequency sheds light on its influence on rotor behavior under varying operational conditions.

Figure 16 delineates the response of rotor displacement across five distinct frequency levels—8 Hz, 9 Hz, 10 Hz, 11 Hz, and 12 Hz. The observed trends offer valuable insights into how frequency variations affect the dynamic behavior of the motor.

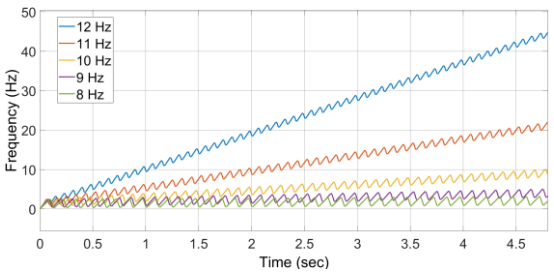

Fig 16. Displacement corresponding to various frequency levels

This behavior in response to frequency variations is predictable given the inherent nature of the piezoelectric motor. As the frequency increases, the number of cycles per unit of time rises proportionally, resulting in a higher duty cycle. This increase in duty cycles directly translates to more frequent interactions between the piezoelectric elements and the rotor, consequently enhancing the motor's actuation and displacement per second.

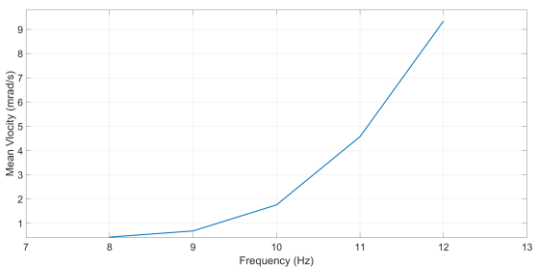

Fig 17. Mean velocity corresponding to various frequency levels

Figure 17 delves into the mean velocity of the motor corresponding to the aforementioned frequency levels. Notably, the ascending trend underscores a non-linear relationship between frequency and motor performance, with a pronounced rate of increase in velocity compared to voltage adjustment

5.3. Friction Coefficient

The friction coefficient emerges as a critical determinant significantly impacting the efficiency and performance of rotary piezoelectric motors.

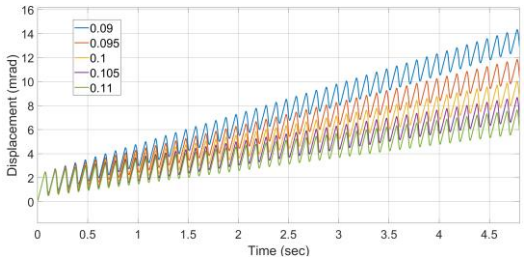

Fig. 18 Displacement corresponding to various μlevels

Figure 18 presents the displacement of the rotor under five different friction coefficient conditions ranging from 0.09 to 0.11. The motor was initially driven at $\mu = 0.1$, and subsequently, the friction coefficient was adjusted by increments and decrements of 10 percent. The results highlight the response of the rotor displacement to variations in the friction coefficient, providing valuable insights into the motor's performance under different friction conditions.

The observed decrease in velocity as the friction coefficient increases is a direct consequence of the fundamental relationship between friction force, preload, and the coefficient of friction. According to Equation 6, this phenomenon arises from an increase in friction force, which is determined by the product of the friction coefficient and preload. As the friction coefficient increases, the slip between the leg and the rotor becomes more challenging. Consequently, during each duty cycle, the slip is reduced because the two surfaces adhere more tightly, amplifying the small backward step in the duty cycle.

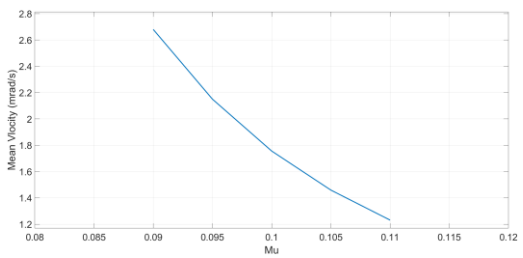

Fig. 19 Mean velocity corresponding to various μlevels

In Figure 19, we illustrate the mean velocity of the motor corresponding to the five different friction coefficient levels. Interestingly, the curve exhibits a decreasing trend as the friction coefficient increases. This observation indicates that higher friction coefficients lead to reduced motor velocity, suggesting that frictional losses play a significant role in limiting motor performance.

5.4. Duty Ratio

Lastly, the duty ratio emerges as a crucial aspect dictating the performance and efficiency of rotary piezoelectric motors.

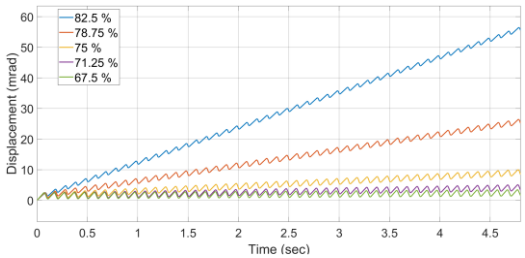

Fig. 20 Displacement corresponding to various duty ratio levels

Figure 20 unveils the response of rotor displacement to diverse $C_{dr} \times e_{dr}$, ranging from 67.5% to 82.5%. These observations underscore the intricate influence of stick and slip times on motor performance.

The noted increase in displacement over time is a direct consequence of the stick-slip phenomenon and the definition of the duty cycle. The stick-slip phenomenon, characterized by alternating periods of sticking (where the rotor is stationary relative to the stator) and slipping (where the rotor moves), plays a pivotal role in the motor's performance.

As the duty ratio increases, the duration of the stick phase is extended, resulting in greater forward motion of the motor. This is because longer stick times allow for more significant energy transfer from the stator to the rotor, thereby enhancing displacement. Conversely, shorter stick times lead to reduced forward motion, as the energy transfer is less efficient.

Moreover, the duty cycle's impact on motor velocity is evident from the data presented in Figure 21. Higher duty ratios correlate with increased overall velocity due to the prolonged stick times, which minimize backward motion and maximize forward displacement. This relationship highlights the importance of optimizing the duty ratio to achieve desired performance characteristics in rotary piezoelectric motors.

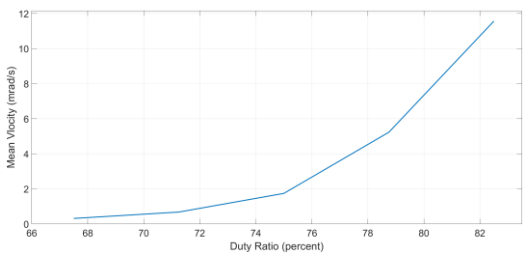

Fig. 21 Mean velocity corresponding to various duty ratio levels

Figure 21 highlights the direct relationship between duty ratio and motor velocity, with higher duty ratios correlating to enhanced overall velocity due to increased stick times and reduced backward motion.

5.5. Compression of parameters

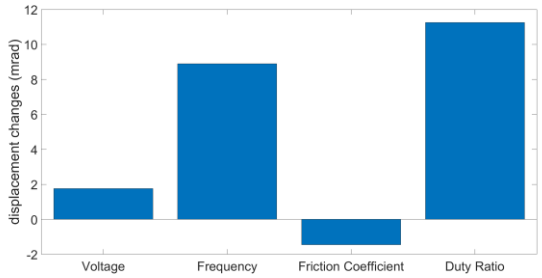

Fig. 22 Compression between different parameters

To assess the sensitivity of various parameters, all factors are presented in Figure 22. Within this figure, the effects of a 20 percent change in each parameter are illustrated. As depicted, the duty ratio emerges as the most influential parameter, followed closely by frequency. Subsequently, voltage demonstrates a significant impact, whereas friction coefficient emerges as the sole parameter exhibiting a consistent decrease across all variations.

6. Conclusion

In conclusion, this article embarked on a comprehensive investigation of piezoelectric motors, commencing with an extensive review of prior research endeavors encompassing diverse motor types. Subsequently, a preliminary iteration of a rotational piezomotor was meticulously fabricated, enabling the acquisition of empirical data. Leveraging the dynamics of the problem, a mathematical model was formulated, and through systematic identification of the system, its associated parameters were ascertained. Consequently, a comparative analysis was conducted, scrutinizing the disparities between the experimental and theoretical data. Remarkably, the adoption of LuGre friction within the forward model yielded a root mean square error (RSME) parameter that exhibited an approximate six-fold enhancement compared to the utilization of Colomb friction in a previous study. With the validation of model accuracy, a sensitivity analysis was undertaken to unravel the model's responsiveness to parameter variations. This involved manipulating the parameters within a 10% higher and 10% lower range. The scrutinized parameters encompassed voltage, frequency, friction coefficient, and duty ratio. Notably, it was deduced that the duty ratio parameter exerted the most profound influence on the output parameter, namely, the rotational speed of the rotor, while frequency and voltage occupied the secondary and tertiary positions, respectively. An essential finding from this research is the inverse relationship between the friction coefficient and the rotational speed of the piezoelectric motor. Moving forward, it is recommended to extend the examination of the proposed model to encompass a broader frequency range. Furthermore, exploring the sensitivity of additional parameters, such as contact angle and the geometric configuration of the flexible mechanism, on the performance of the piezoelectric motor is highly encouraged.

References

[1] Mohith S, Upadhya AR, Navin KP, Kulkarni SM, Rao M. Recent trends in piezoelectric actuators for precision motion and their applications: A review. Smart Materials and Structures. 2020 Dec 1;30(1):013002.

[2] Shome SK, Datta U, Mukherjee A, Bhattacharjee P. Piezoelectric actuation and motors: An overview of nonlinearities, control, and emerging industrial applications. 2018 3rd International Innovative Applications of Computational Intelligence on Power, Energy and Controls with their Impact on Humanity (CIPECH). 2018 Nov 1:1-5.

[3] Xu D, Liu Y, Shi S, Liu J, Chen W, Wang L. Development of a nonresonant piezoelectric motor with nanometer resolution driving ability. IEEE/ASME Transactions on Mechatronics. 2018 Jan 8;23(1):444-51.

[4] Mirshamsi M, Rafeeyan M. QFT control of a two-link rigid-flexible manipulator. IFAC Proceedings Volumes. 2010 Jan 1;43(21):274-81.

[5] Spanner K. Survey of the various operating principles of ultrasonic piezomotors. InProceedings of the 10th International Conference on New Actuators 2006 Jun.

[6] Peng Y, Peng Y, Gu X, Wang J, Yu H. A review of long range piezoelectric motors using frequency leveraged method. Sensors and Actuators A: Physical. 2015 Nov 1;235:240-55.

[7] Deng J, Liu Y, Liu J, Xu D, Wang Y. Development of a planar piezoelectric actuator using bending–bending hybrid transducers. IEEE Transactions on Industrial Electronics. 2018 Oct 10;66(8):6141-9.

[8] Li J, Huang H, Morita T. Stepping piezoelectric actuators with large working stroke for nano-positioning systems: A review. Sensors and Actuators A: Physical. 2019 Jun 15;292:39-51.

[9] Zhou H, Henson B, Bell A, Blackwood A, Beck A, Burn R. Linear piezo-actuator

and its applications. University of Leeds. 2001.

[10] Gao Y, Wen J, Ma J, Zhang Y, Wang R, Hu Y, Li J. A self-adapting linear inchworm piezoelectric actuator based on a permanent magnets clamping structure. Mechanical systems and signal processing. 2019 Oct 1;132:429-40.

[11] Headings LM. Modeling, characterization, and design of smart material driven stick-slip actuation mechanisms (Master's thesis, The Ohio State University).

[12] Lu X, Gao Q, Gao Q, Yu Y, Zhang X, Qiao G, Zhao H, Cheng T. Design, modeling, and performance of a bidirectional stick-slip piezoelectric actuator with coupled asymmetrical flexure hinge mechanisms. Journal of Intelligent Material Systems and Structures. 2020 Oct;31(17):1961-72.

[13] Yang S, Li Y, Xia X, Ning P, Ruan W, Zheng R, Lu X. A topology optimization method and experimental verification of piezoelectric stick-slip actuator with a flexure hinge mechanism. Archive of Applied Mechanics. 2022 Jan 1:1-5.

[14] Fernandez JM, Perriard Y. Sensitivity analysis and optimization of a standing wave ultrasonic linear motor. ieee transactions on ultrasonics, ferroelectrics, and frequency control. 2006 Jul;53(7):1352-61.

[15] Dong Z, Yang M. Optimal design of a double-vibrator ultrasonic motor using combination method of finite element method, sensitivity analysis and adaptive genetic algorithm. Sensors and Actuators A: Physical. 2017 Oct 15;266:1-8.

[16] Tiemin Z, Fei C, Shenghua L, Li L, Sheng W. FEM analysis and parameter optimization of a linear piezoelectric motor macro driven. InIntelligent Robotics and Applications: 7th International Conference, ICIRA 2014, Guangzhou, China, December 17-20, 2014, Proceedings, Part I 7 2014 (pp. 171-178). Springer International Publishing.

[17] Flueckiger M, Fernandez JM, Perriard Y. Finite element method based design and optimisation methodology for piezoelectric ultrasonic motors. Mathematics and Computers in Simulation. 2010 Oct 1;81(2):446-59.

[18] Johanastrom K, Canudas-De-Wit C. Revisiting the LuGre friction model. IEEE Control systems magazine. 2008 Nov 17;28(6):101-14.

[19] PiezoDrive, "Piezoelectric Motors," PiezoDrive. [Online]. Available: https://www.piezodrive.com. [Accessed: Aug. 5, 2024]

[20] Azadkhani M, Ghafarirad H, Zareinejad M. Design, Modeling and Implementation of Rotary Piezoelectric Motor. In2023 11th RSI International Conference on Robotics and Mechatronics (ICRoM) 2023 Dec 19 (pp. 728-732). IEEE.

Biography

Mohammad Azadkhani is currently MSc. Student in mechanical engineering at Amirkabir University of Technology (AUT), Tehran, Iran and He received his BSc. Degree in from K.N. Toosi University of Technology. His research interest includes vibrations, piezoelectric materials and multi-physics problems.

Fatemeh Karimi is currently MSc. Student in mechanical engineering at Amirkabir University of Technology (AUT), Tehran, Iran. Her research interest includes mechatronics and smart materials.

Hamed Ghafarirad received Ph.D. degree in mechanical engineering from Amirkabir University of Technology (AUT), Tehran, Iran, in 2014. He is an Associate Professor of Mechanical Engineering Department at AUT since 2015. His research interests include mechatronics, robotics, microrobotics and smart materials.

Mohammad Zareinejad received the B.S., M.S., and Ph.D. degrees in mechanical engineering from Amirkabir University of Technology, Tehran, Iran, in 2003, 2005, and 2009, respectively. He is currently an Assistant Professor of Mechanical Engineering at the Department of Mechanical Engineering, Amirkabir University of Technology, Tehran, Iran, where he also directs the Mechatronics Laboratory. His research interests include soft robotics and fluid power.